MRS Communications (2013), 3, 225–233
© Materials Research Society, 2013
doi:10.1557/mrc.2013.41

MRS Communications

Research Letters

Oxygen-permeable membrane materials based on solid or liquid Bi_2O_3

Valery V. Belousov, A.A. Baikov Institute of Metallurgy and Materials, Russian Academy of Sciences, 49 Leninskii Pr., 119991 Moscow, Russia
Address all correspondence to Valery V. Belousov at **vbelousov@imet.ac.ru**

(Received 5 August 2013; accepted 27 September 2013)

Abstract

Most important advances of the last years in research and development of oxygen ion transport membrane (ITM) materials based on solid or liquid Bi_2O_3 are briefly given. Special attention is paid to the transport properties of novel NiO/δ-Bi_2O_3 and In_2O_3/δ-Bi_2O_3 ceramic and ZnO/Bi_2O_3 solid/liquid composites. These composites show promise for use as ITM with the oxygen permeation rate comparable with that of the state-of-the-art membrane materials. The in situ Bi_2O_3 melt crystallization and grain boundary wetting methods of formation of the gas-tight composites are considered.

Introduction

Gas-tight ceramic or solid/liquid metal oxide composites exhibiting high mixed conductivity could be used as ion transport membranes, ITM, for oxygen separation from air.[1–5] The advantages of oxygen separation by ITM over technologies such as pressure- and temperature-swing adsorption and porous membrane separation methods[6–9] is their infinite separation factor. The composite ITM are usually made from electron- and ion-conducting chemically compatible and thermodynamically stable metal oxides. In an electrochemical field, the high ambipolar conductivity of oxygen ions and electrons results in the high oxygen permeation rate (Fig. 1). The oxygen permeation flux through ITM depends on three mechanisms: the first is the dissociation of oxygen molecules into oxygen anions at the membrane surface, known as surface exchange kinetics.[10] The second is the migration of oxygen anions through the membrane,[11] while the third is the recombination of oxygen anions back to oxygen molecules on the other side of the membrane. Each mechanism has the potential to become the rate-limiting step.

Bismuth oxide exists as four crystallographic polymorphs.[12–18] The room temperature α-Bi_2O_3 is monoclinic. It transforms at 730 °C into the face-centered cubic (fcc) δ-Bi_2O_3, which is stable up to the melting point at 820 °C.[13,14] On cooling, large thermal hysteresis occurs and the metastable tetragonal β or body-centered cubic (bcc) γ form can be obtained, depending on the cooling conditions, transforming to the β-phase at 650 °C or the γ-phase at 639 °C.[15–17] The β-phase transforms to the α-phase at 303 °C, and the γ-phase at 500 °C, although the γ-phase may persist to room temperature with slow cooling rates.[12,18] The α-monoclinic and γ-bcc forms are semiconductors, whereas the β-tetragonal and δ-fcc forms are oxide ion conductors. The δ-phase has the highest known oxygen ionic conductivity. The high ionic conductivity is caused by the large number of oxygen vacancies and high anion mobility. The high concentration of oxygen vacancies is a result of obtaining the fluorite structure with a Bi^{3+} cation. The high anion mobility is related to the high polarizability of the Bi^{3+} cation with its lone pair of electrons.

Ordering of the oxygen vacancies in a monoclinic α-Bi_2O_3 is established.[16,17] On heating trough 730 °C, a first-order α → δ-Bi_2O_3 transition is a vacancy order-disorder transition. The transition enthalpy is 2.7 times the heat of melting. The entropy gain is 75% of the total entropy gain on passing from the solid to the liquid state. The transition corresponds to a disordering of the anion sublattice,[18] which results in an abrupt increase of the oxygen ionic conductivity. However, one major problem of using δ-Bi_2O_3 as the oxygen ionic conductor in composite ITM is their cracking due to the volume change (~11–12%) associated with polymorphic transformation of the monoclinic α- into cubic δ-Bi_2O_3 at the ITM heating. The δ-phase can be stabilized, but the ionic conductivity is substantially reduced.[19–27] Recently this problem is alleviated. The in situ Bi_2O_3 melt crystallization and grain boundary wetting

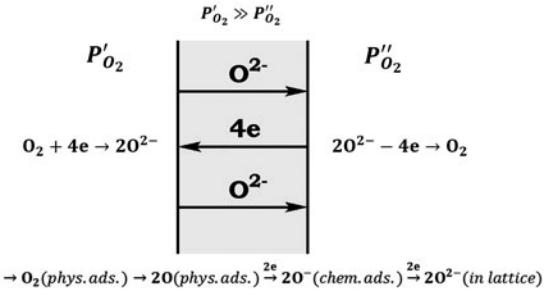


Figure 1. Schematic of oxygen ion and electron transport through ITM.

https://doi.org/10.1557/mrc.2013.41 Published online by Cambridge University Press

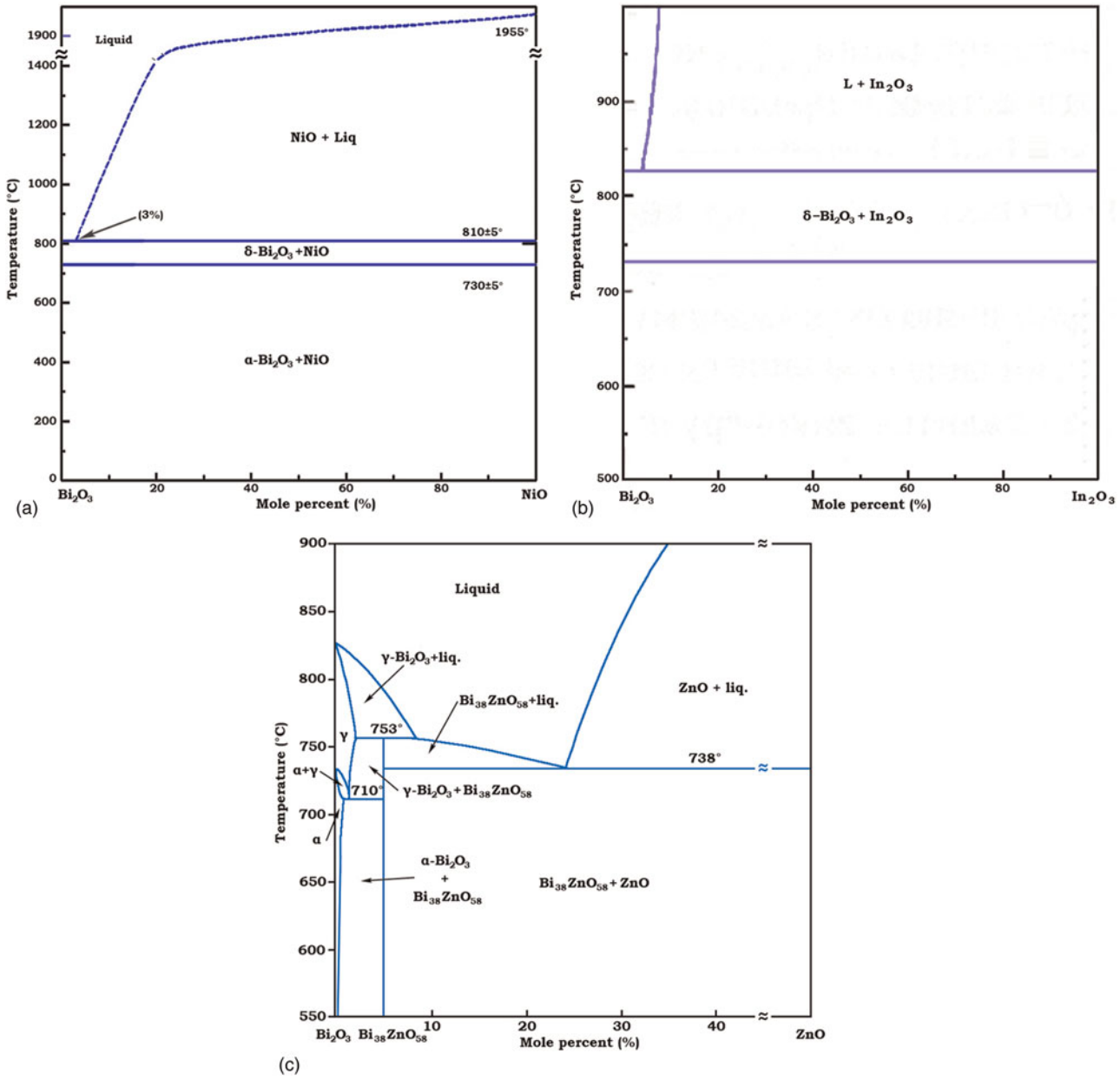


Figure 2. Phase diagrams of (a) Bi_2O_3–NiO,[35] (b) Bi_2O_3–In_2O_3,[36] and (c) Bi_2O_3–ZnO.[37]

methods of formation of the gas-tight NiO/δ-Bi_2O_3 and In_2O_3/δ-Bi_2O_3 ceramic and ZnO/Bi_2O_3 solid/liquid composites are developed, respectively.[28–30] These composites show the oxygen permeation rate comparable with that of the state-of-the-art membrane materials[31–34] and could be used as ITM for oxygen separation from air. The aim of this paper is to summarize and discuss data on formation methods and transport properties of these composites. Some focus is directed to our own work.

Formation methods

The gas-tight NiO/δ-Bi_2O_3 and In_2O_3/δ-Bi_2O ceramic composites were prepared by the in situ Bi_2O_3 melt crystallization method.[28,29] The previously sintered NiO–54 wt.% Bi_2O_3 and In_2O_3–55 wt.% Bi_2O_3 ceramic composites were then heated to 840 °C. This temperature, according to the NiO–Bi_2O_3 and In_2O_3–Bi_2O_3 phase diagrams [Figs. 2(a) and 2(b)], corresponds to the two-phase area, where the solid NiO or In_2O_3 and liquid are in equilibrium (liquid-phase sintering[38]). After holding at 840 °C for 10–15 min, the composites were slowly (1–5 °C/min) cooled to 800 °C. This temperature corresponds to the two-phase area, where the solid NiO or In_2O_3 and δ-Bi_2O_3 are in equilibrium [Figs. 2(a) and 2(b)]. To avoid the polymorphic transformations of Bi_2O_3, in situ oxygen permeation measurements were performed at 800 °C by gas flow

https://doi.org/10.1557/mrc.2013.41 Published online by Cambridge University Press

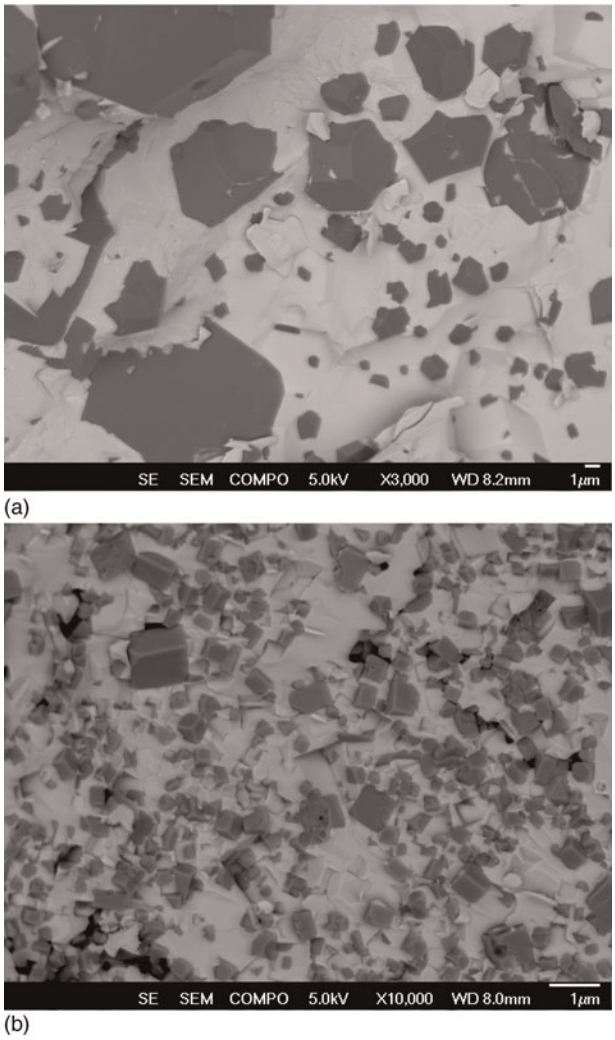


Figure 3. Scanning electron micrographs of fractures of (a) NiO–54 wt.% Bi_2O_3 and (b) In_2O_3–55 wt.% Bi_2O_3 composites after cooling from 840 °C; dark constituent is NiO or In_2O_3, respectively.

technique.[4] Microstructure of the composites is presented in Fig. 3.

The gas-tight ZnO/Bi_2O_3 solid/liquid composites were prepared by the grain boundary wetting method.[30] The previously sintered ZnO – 15, 20, 25, and 30 wt.% Bi_2O_3 ceramic composites were then heated to 760–820 °C. This temperature range corresponds to the two-phase area, where the solid ZnO and liquid are in equilibrium [Fig. 2(c)]. During the heating, grain boundary wetting transition occurred. The grain boundary wetting transition has been established at eutectic point in Bi_2O_3-containing ceramic composites.[39–49] The result is a solid/liquid composite consisting of ZnO solid grains and liquid channels at the grain boundaries (Fig. 4). This is called a liquid-channel grain-boundary structure (LGBS).[3,4,50,51] The intergranular liquid channels give the LGBS high mechanical plasticity[52]

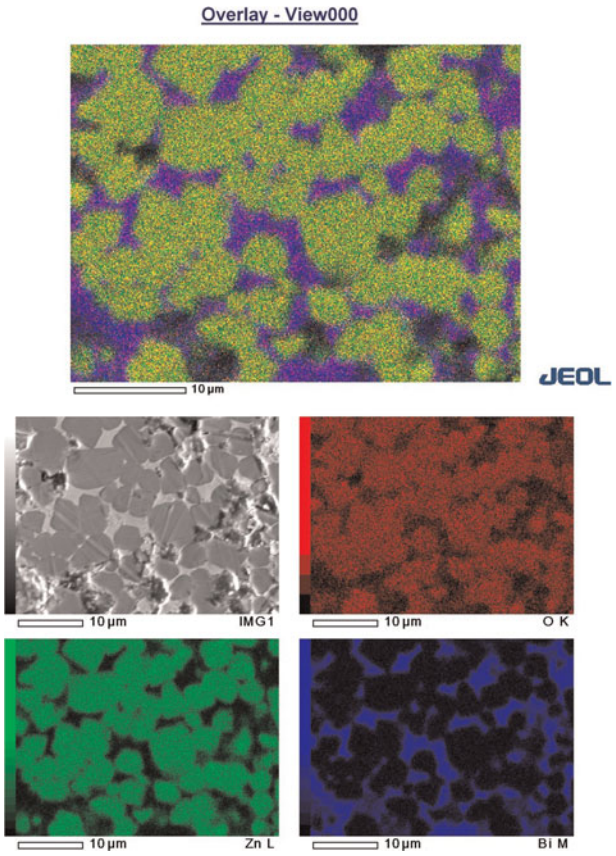


Figure 4. Scanning electron micrograph of polished cross-section of ZnO–30 wt.% Bi_2O_3 composite after cooling from 800 °C; dark constituent in IMG1 is ZnO.

(Fig. 5), which would make it easy to shape and alleviate problems due to brittleness.

Transport properties

NiO/δ-Bi_2O_3 and In_2O_3/δ-Bi_2O_3 ceramic composites

Transport properties of NiO–54 wt.% Bi_2O_3 and In_2O_3–55 wt.% Bi_2O_3 ceramic composites are reported in Refs.[28,29] Temperature dependences of conductivities of these composites are presented in Fig. 6 (temperature dependences of NiO, In_2O_3, and Bi_2O_3 conductivities for comparison). In the temperature range of 500–730 °C, contribution of In_2O_3 or NiO electron or hole conductivity, respectively, is considerable.[53–56] The conductivity jump at 730 °C induced by $\alpha \rightarrow \delta$-$Bi_2O_3$ polymorphic transformation was accompanied by increasing oxygen ionic conductivity. The defect chemistry models are proposed to explain the ionic conductivity of δ-Bi_2O_3.[57–65]

Figure 7 shows the oxygen permeation fluxes through NiO–54 wt.% δ-Bi_2O_3 and In_2O_3–55 wt.% δ-Bi_2O_3 ceramic composites as a function of oxygen partial pressure difference $\lg(P'_{O_2}/P''_{O_2})$ between oxygen-rich and -lean sides of the composites. Wagner's Eq. (1) is usually used to describe the oxygen

https://doi.org/10.1557/mrc.2013.41 Published online by Cambridge University Press

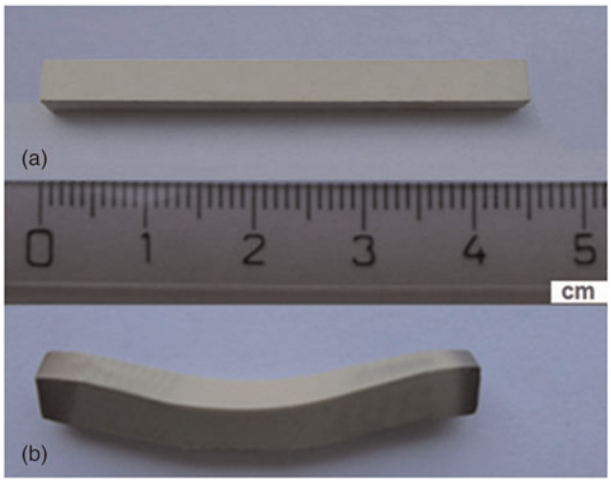


Figure 5. Photography of (a) starting ZnO–30 wt.% Bi_2O_3 ceramic composite and (b) ZnO–30 wt.% Bi_2O_3 LGBS after deformation at 800 °C.

permeation flux (j_{O_2}) due to the bulk chemical diffusion[66]

$$j_{O_2} = \frac{RT}{16F^2L}\int_{\ln P''_{O_2}}^{\ln P'_{O_2}} \sigma_{amb} \mathrm{d} \ln P_{O_2}, \quad (1)$$

$$\sigma_{amb} = \frac{\sigma_i \sigma_e}{\sigma_i + \sigma_e}, \quad (2)$$

where σ_{amb}, σ_i, and σ_e are the ambipolar, ionic, and electronic conductivities, respectively, L is the membrane thickness, F is the Faraday constant, R is the universal gas constant, and T is the temperature. Taking an average value of σ_{amb} simplifies

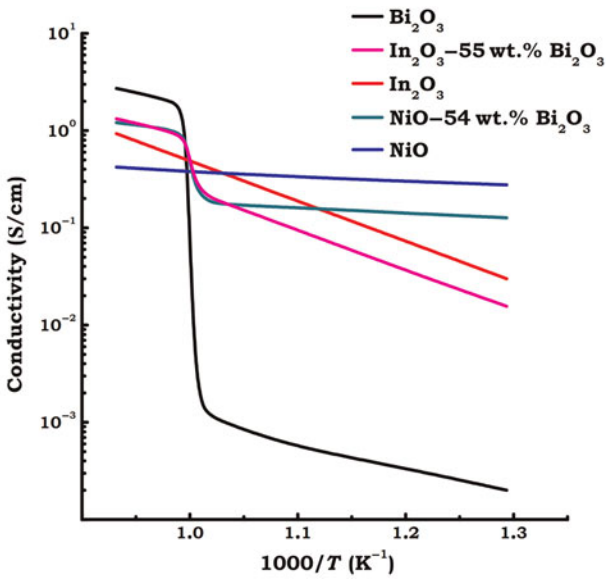


Figure 6. Temperature dependences of conductivities of NiO–54 wt.% Bi_2O_3, In_2O_3–55 wt.% Bi_2O_3, NiO, In_2O_3, and Bi_2O_3. S = Siemens.

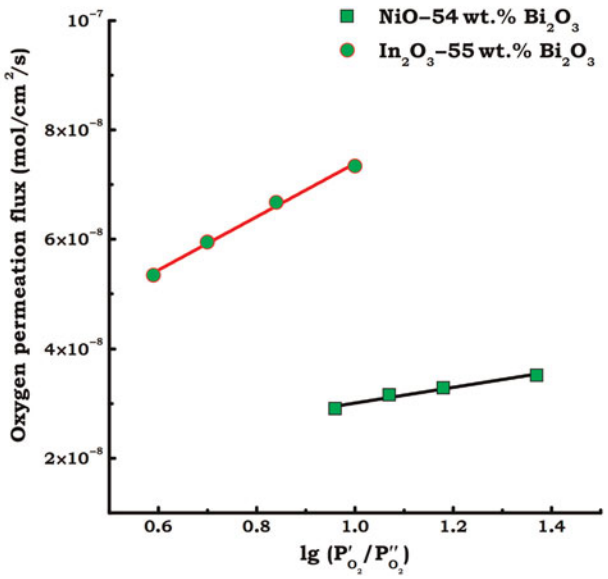


Figure 7. Dependences of oxygen permeation fluxes through NiO–54 wt.% Bi_2O_3 (thickness 2.5 mm) and In_2O_3–55 wt.% Bi_2O_3 (thickness 2.9 mm) ceramic composites on oxygen partial pressure difference at 800 °C.

Eq. (1) further so that j_{O_2} is proportional to $\overline{\sigma_{amb}}$ and P'_{O_2} / P''_{O_2}

$$j_{O_2} = \frac{RT}{16F^2L}\overline{\sigma_{amb}} \ln \frac{P'_{O_2}}{P''_{O_2}}. \quad (3)$$

The calculated by Eq. (3) and the experimental values of oxygen permeation fluxes are of the same order of magnitude (Table 1), which shows that (in the range of composite thickness 2.5–2.9 mm used in the present study) the oxygen permeation rate is controlled by ambipolar conductivity.

ZnO–15, 20, 25, and 30 wt.% Bi_2O_3 solid/liquid composites

Transport properties of ZnO–15, 20, 25, and 30 wt.% Bi_2O_3 LGBS are reported in Ref.[30] Temperature dependences of conductivities of these composites are presented in Fig. 8. According to the ZnO–Bi_2O_3 phase diagram [Fig. 2(c)], the $Bi_{38}ZnO_{58}$ compound is in the temperature range of 600–753 °C. In this temperature range, contribution of $Bi_{38}ZnO_{58}$ electron conductivity is considerable. The conductivity enhancement at 753 °C was caused by LGBS formation (Fig. 4). At the LGBS formation, contribution of oxygen ionic conductivity comes significant. The intergranular liquid channels can serve as conduction pathways for oxygen ions.[3] The oxygen ionic conductivity of LGBS will be increased with Bi_2O_3 content.

The liquid volume fraction dependences of the LGBS oxygen ion transference number are presented in Fig. 9. The oxygen ion transference number increases with volume fraction of liquid. The LGBS is a mixed conductor, where the

https://doi.org/10.1557/mrc.2013.41 Published online by Cambridge University Press

Table 1. Experimental ($j_{O_2}^{exp}$) and calculated ($j_{O_2}^{theor}$) values of the oxygen permeation fluxes through NiO–54 wt.% Bi_2O_3 and In_2O_3–55 wt.% Bi_2O_3 ceramic composites.

Composite	L (cm)	P'_{O_2} (atm)	P''_{O_2} (atm)	σ_{amb} ($\Omega^{-1} \cdot cm^{-1}$)	σ_e ($\Omega^{-1} \cdot cm^{-1}$)	σ_i ($\Omega^{-1} \cdot cm^{-1}$)	$j_{O_2}^{exp}$ [mol/(cm^2 · s)]	$j_{O_2}^{theor}$ [mol/(cm^2 · s)]	T (K)	η
NiO–54 wt.% Bi_2O_3	0.25	0.21	0.023	0.182	0.210	1.355	2.91×10^{-8}	9.87×10^{-8}	1073	0.5
In_2O_3–55 wt.% Bi_2O_3	0.29	0.21	0.054	0.346	0.465	1.355	5.34×10^{-8}	9.67×10^{-8}	1073	0.5

$\sigma_i = \eta\sigma_{Bi_2O_3}$; $\sigma_e = (1 - \eta)\sigma_{NiO\ (or\ In_2O_3)}$; η is the volume fraction of Bi_2O_3; $\sigma_{Bi_2O_3}$, $\sigma_{In_2O_3}$, and σ_{NiO} are the conductivities of Bi_2O_3, In_2O_3, and NiO, respectively (Fig. 6).

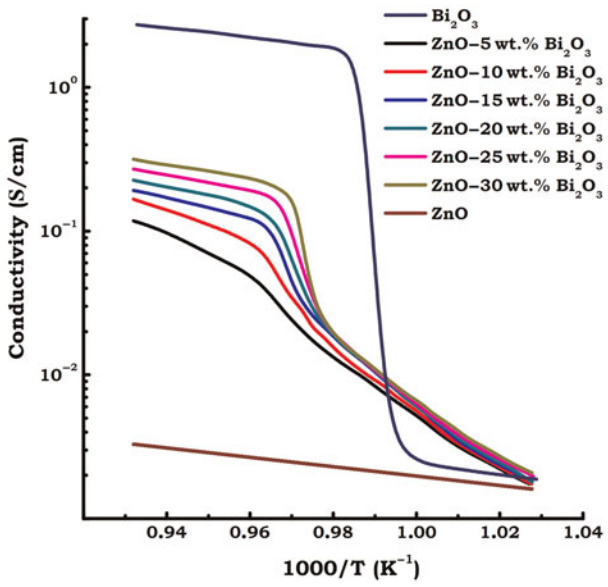


Figure 8. Temperature dependences of conductivities of ZnO–15, 20, 25, and 30 wt.% Bi_2O_3, ZnO, and Bi_2O_3. S = Siemens.

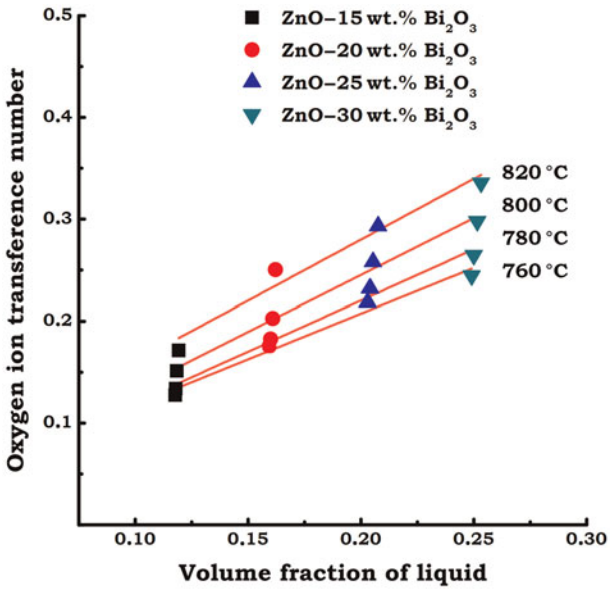


Figure 9. Liquid volume fraction dependences of oxygen ion transference number of ZnO–15, 20, 25, and 30 wt.% Bi_2O_3 LGBS.

intergranular liquid channels can conduct both the oxygen ions and electrons[67] and the solid grains of ZnO conduct the electrons.[68,69]

Figures 10 and 11 show the oxygen permeation fluxes through LGBS as a function of oxygen partial pressure difference and volume fraction of liquid, respectively. The oxygen permeation flux increases with volume fraction of liquid. As the volume fraction of liquid is in direct proportion to the Bi_2O_3 content [Fig. 2(c)], the oxygen permeation flux through LGBS increases with Bi_2O_3 content.

The calculated by Eq. (3) and the experimental values of oxygen permeation fluxes are of the same order of magnitude (Table 2), which shows that (at the LGBS thickness approximately 2 mm used in the present study) the oxygen permeation rate is controlled by ambipolar conductivity.

Prospects

In order to compare the membrane material performances, the oxygen permeability ($j^*_{O_2}$) was calculated by Eq. (4):

$$j^*_{O_2} = j_{O_2} \frac{L}{\ln(P'_{O_2}/P''_{O_2})}. \quad (4)$$

The values of oxygen permeability of In_2O_3–55 wt.% δ-Bi_2O_3 and NiO–54 wt.% δ-Bi_2O_3 ceramic composites and ZnO–30 wt.% Bi_2O_3 LGBS are comparable with that of the perovskite-type membrane materials (Table 3). However, the high oxygen permeability is just one of many material properties that are important for the ITM. The membrane material must combine good permeability with other properties such as high strength,

https://doi.org/10.1557/mrc.2013.41 Published online by Cambridge University Press

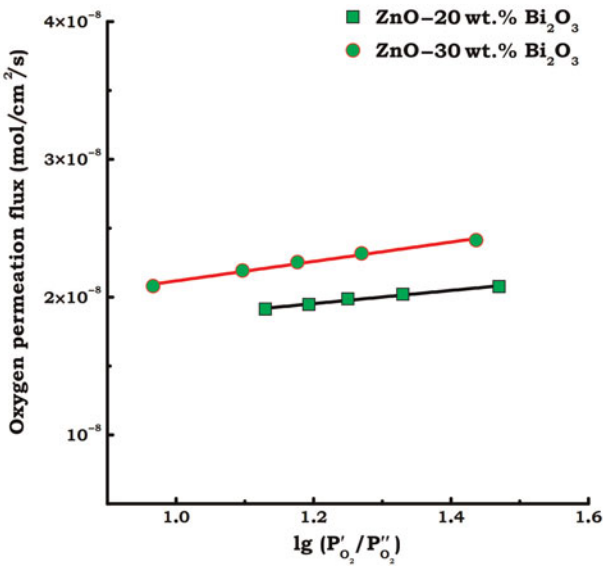


Figure 10. Dependences of oxygen permeation fluxes through ZnO–20 and 30 wt.% Bi_2O_3 LGBS (thickness 1.7 and 1.9 mm, respectively) on oxygen partial pressure difference at 800 °C.

low (or linear) thermal expansion, high resistance to reaction with CO_2, etc.[1,77–79]

Plastic LGBS materials are developing as an alternative to the brittle ceramic membrane materials. In order to assess the potential of LGBS as ITM, it is necessary to understand their ionic and electronic conductivities and how these, and their mechanical properties, are related to their composition and microstructure.

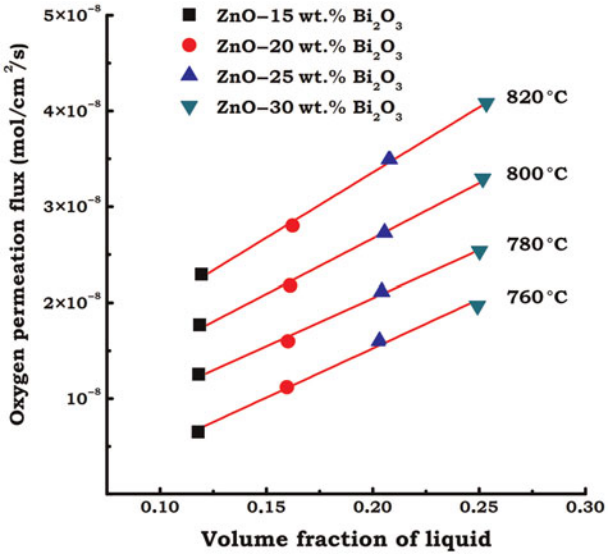


Figure 11. Liquid volume fraction dependences of oxygen permeation fluxes through ZnO–15, 20, 25, and 30 wt.% Bi_2O_3 LGBS (thickness approximately 2 mm); P_{O_2} = 0.21 atm and P'_{O_2} = 0.005 atm.

Table 2. Experimental ($j_{O_2}^{exp}$) and calculated ($j_{O_2}^{theor}$) values of the oxygen permeation fluxes through ZnO–20 and 30 wt.% Bi_2O_3 LGBS.

Composite	L (cm)	P_{O_2} (atm)	P'_{O_2} (atm)	σ_{amb} ($\Omega^{-1} \cdot cm^{-1}$)	σ_e (Ω^{-1}/cm^1)	σ_i ($\Omega^{-1} \cdot cm^{-1}$)	$j_{O_2}^{exp}$ [mol/(cm^2 · s)]	$j_{O_2}^{theor}$ [mol/(cm^2 · s)]	T (K)
ZnO–20 wt.% Bi_2O_3 LGBS	0.17	0.21	0.0071	0.037	0.181	0.046	2.08×10^{-8}	4.36×10^{-8}	1073
ZnO–30 wt.% Bi_2O_3 LGBS	0.19	0.21	0.0077	0.066	0.222	0.094	2.41×10^{-8}	6.89×10^{-8}	1073

$\sigma_i = t_i\sigma$; $\sigma_e = (1 - t_i)\sigma$; t_i, is the oxygen ion transference number of composite (Fig. 9); σ is the conductivity of composite (Fig. 8).

https://doi.org/10.1557/mrc.2013.41 Published online by Cambridge University Press

Table 3. The oxygen permeability ($j^*_{O_2}$) of same membrane materials.

Membrane material	T (K)	j_{O_2} [mol/(cm^2 · s)]	L (mm)	P'_{O_2} (atm)	P''_{O_2} (atm)	$j^*_{O_2}$ [mol/(cm · s)]	References
$Ba_{0.5}Sr_{0.5}Zn_{0.2}Fe_{0.8}O_{3-\delta}$	1073	1.1×10^{-6}	1.45	0.21	0.010	5.2×10^{-8}	[70]
$Ba_{0.5}Sr_{0.5}Co_{0.8}Fe_{0.2}O_{3-\delta}$	1073	7.9×10^{-7}	1.0	0.21	0.067	7.0×10^{-8}	[71]
$La_{0.6}Sr_{0.4}Co_{0.8}Fe_{0.2}O_{3-\delta}$	1123	5.6×10^{-8}	0.75	0.21	0.001	7.9×10^{-10}	[72]
$SrCo_{0.8}Fe_{0.2}O_{3-\delta}$	1073	1.8×10^{-7}	1.0	0.21	0.067	1.6×10^{-9}	[73]
$SrCo_{0.95}Ti_{0.05}O_{3-\delta}$	1153	4.5×10^{-7}	1.4	0.21	0.084	6.9×10^{-8}	[74]
$Sr_{0.7}Gd_{0.3}CoO_{3-\delta}$	1153	4.1×10^{-8}	1.4	0.21	0.084	6.3×10^{-9}	[74]
$Sr_{0.7}La_{0.3}CoO_{3-\delta}$	1153	2.6×10^{-7}	1.4	0.21	0.084	4.0×10^{-8}	[74]
$Sr_{0.7}Nd_{0.3}CoO_{3-\delta}$	1153	1.6×10^{-7}	1.4	0.21	0.084	2.4×10^{-8}	[74]
$Sr_{0.7}Sm_{0.3}CoO_{3-\delta}$	1153	1.0×10^{-7}	1.4	0.21	0.084	1.5×10^{-8}	[74]
$Y_{0.1}Ba_{0.9}CoO_{3-\delta}$	1173	2.7×10^{-7}	2.0	0.21	0.0001	7.1×10^{-9}	[75]
$La_{0.4}Ba_{0.6}Co_{0.2}Fe_{0.8}O_{3-\delta}$	1173	3.4×10^{-7}	2.3	1.0	0.0002	9.2×10^{-9}	[76]
NiO–54 wt.%Bi_2O_3	1073	3.5×10^{-8}	2.5	0.21	0.0084	2.7×10^{-9}	
In_2O_3–55 wt.%Bi_2O_3	1073	5.3×10^{-8}	2.9	0.21	0.054	1.1×10^{-8}	
ZnO–30 wt.%Bi_2O_3 LGBS	1073	2.4×10^{-8}	1.9	0.21	0.0077	1.4×10^{-9}	

The development of materials with dimensions in the nanoscale range is a highly active area of research, because they often have different properties from the bulk materials. Restructuring simple ionic crystals at the nanoscale can alter their electrical properties.[80] In this connection, it is interesting to study the transport properties of liquid-channel grain-boundary nanostructures[81] where the solid/liquid interfaces can contribute significantly in ionic conduction.[40]

Acknowledgment

We thank RFBR and Presidium of the RAS for financial support.

References

1. A.C. Bose, G.J. Stiegel, P.A. Armstrong, B.J. Halper, and E.P. Foster: Progress in ion transport membranes for gas separation application, In *Inorganic Membranes for Energy and Environmental Application*, A.C. Bose, ed. (Springer, New York, USA, 2009) p. 3, 26.
2. X. Zhu and W. Yang: Composite membrane based on ionic conductor and mixed conductor for oxygen separation. *AIChE J.* **54**, 665 (2008).
3. V.V. Belousov and S.V. Fedorov: Accelerated mass transfer involving the liquid phase in solids. *Russ. Chem. Rev.* **81**, 44 (2012).
4. S.V. Fedorov, V.V. Belousov, and A.V. Vorobiev: Transport properties of $BiVO_4$ – V_2O_5 liquid-channel grain-boundary structures. *J. Electrochem. Soc.* **155**, F241 (2008).
5. V.V. Belousov, S.V. Fedorov, and A.V. Vorobiev: The oxygen permeation of solid/melt composite $BiVO_4$ – 10 wt.% V_2O_5 membrane. *J. Electrochem. Soc.* **158**, B601 (2011).
6. W.H. Isalski: *Separation of Gases* (Clarendon Press, Oxford, 1989).
7. R.T. Yang: *Gas Separation by Adsorption Processes* (Butterworth, Boston, 1987).
8. H.P. Hsieh: New membrane materials and processes for separation. AIChE Symposium Series, No 261, v. 84, 1988 (edited by K.K. Sirkar and D.R. Lloyd).
9. N. Toshima and H. Asanuma: Porous Polymer Complexes for Gas Separation (chapter 5). Polymers for gas separation, N. Toshima, ed. (VCH, Weinheim, 1992).
10. H.J.M. Bouwmeester, H. Kruidhof, and A.J. Burggraaf: Importance of the surface exchange kinetics as rate-limiting step in oxygen permeation through mixed-conducting oxides. *Solid State Ion.* **72**, 185 (1994).
11. B.A. Van Hassel: Oxygen transfer across composite oxygen transport membranes. *Solid State Ion.* **174**, 253 (2004).
12. H.A. Harwig and A.G. Gerards: Electrical properties of the α, β, γ, and δ phases of bismuth sesquioxide. *J. Solid State Chem.* **26**, 265 (1978).
13. P.D. Battle, C.R.A. Catlow, J. Drennan, and A.D. Murry: The structure and properties of the oxygen conducting δ phase of Bi_2O_3. *J. Phys.* C 16, L561 (1983).
14. P.D. Battle, C.R.A. Catlow, A.V. Chadwick, P. Cox, G.N. Greaves, and L.M. Moroney: Sesquioxides with the fluorite structure. *J. Solid State Chem.* **63**, 8 (1986).
15. S.K. Blower and C. Graves: The structure of γ-Bi_2O_3 from powder neutron diffraction data. *Acta Crystallogr.* **C44**, 587 (1988).
16. H.A. Harwig: On the structure of bismuth sesquioxide: α-, β-, γ-, and δ- phase. *Z. Anorg. Allg. Chem.* **444**, 151 (1978).
17. H.A. Harwig and J.W. Weenk: Phase relation in bismuth sesquioxide. *Z. Anorg. Allg. Chem.* **444**, 167 (1978).
18. H.A. Harwig and A.G. Gerards: The polymorphism of bismuth sesquioxide. *Thermochim. Acta* **28**, 121 (1979).
19. N. Jiang and E.D. Wachsman: Structural stability and conductivity of phase-stabilized cubic bismuth oxide. *J. Am. Ceram. Soc.* **82**, 3057 (1999).
20. T. Takahashi, H. Iwahara, and T. Arao: High oxide ion conduction in sintered oxide of the Bi_2O_3-Y_2O_3 system. *J. Appl. Electrochem.* **5**, 187 (1975).
21. T. Takahashi, T. Esaka, and H. Iwahara: High oxide ion conduction in sintered oxide of the Bi_2O_3-Gd_2O_3 system. *J. Appl. Electrochem.* **5**, 197 (1975).

https://doi.org/10.1557/mrc.2013.41 Published online by Cambridge University Press

22. M.J. Verker and A.J. Burggraaf: High oxide ion conduction in sintered oxide of the Bi_2O_3-Dy_2O_3 system. *J. Electrochem. Soc.* **128**, 75 (1981).
23. E.D. Wachsman, G.R. Ball, N. Jiang, and D.A. Stevenson: Structural and defect studies in solid oxide electrolytes. *Solid State Ion.* **52**, 213 (1992).
24. K. Fung and A. Virkar: Phase stability, phase transformation kinetics, and conductivity of Y_2O_3-Bi_2O_3 solid electrolyte containing aliovalent dopants. *J. Am. Ceram. Soc.* **74**, 1970 (1991).
25. T. Takahashi and H. Iwahara: Oxide ion conductors based on bismuth sesquioxide. *Mater. Res. Bull.* **13**, 1447 (1978).
26. E.D. Wachsman, S. Boyapati, M.J. Kaufman, and N. Jiang: Modelling of ordered structures of phase-stabilized cubic bismuth oxide. *J. Am. Ceram. Soc.* **83**, 1964 (2000).
27. N. Jiang, R.M. Buchanan, F.E.G. Henn, D.A. Stevenson, and E.D. Wachsman: Aging phenomenon of stabilized bismuth oxide. *Mater. Res. Bull.* **29**, 247 (1994).
28. V.V. Belousov, V.A. Schelkunov, S.V. Fedorov, I.V. Kulbakin, and A.V. Vorobiev: Oxygen-permeable In_2O_3-55 wt.% δ-Bi_2O_3 composite membrane. *Electrochem. Commun.* **20**, 60 (2012).
29. V.V. Belousov, V.A. Schelkunov, S.V. Fedorov, I.V. Kulbakin, and A. V. Vorobiev: Oxygen-permeable NiO-54 wt.% δ-Bi_2O_3 composite membrane. *Ionics* **18**, 787 (2012).
30. I.V. Kul'bakin, V.V. Belousov, S.V. Fedorov, and A.V. Vorobiev: Solid/melt ZnO–Bi_2O_3 composites as ion transport membranes for oxygen separation. *Mater. Lett.* **67**, 139 (2012).
31. J. Hong, P. Kirchen, and A.F. Ghoniem: Numerical simulation of ion transport membrane reactors: oxygen permeation and transport and fuel conversion. *J. Membr. Sci.* **71–85**, 407–408, (2012) doi:10.1016/j.memsci.2012.03.018.
32. J. Hong, P. Kirchen, and A.F. Ghoniem: Interactions between oxygen permeation and homogeneous-phase fuel conversion on the sweep side of an ion transport membrane. *J. Membr. Sci.* **428**, 309 (2013).
33. M.J. Shin and J.H. Yu: Oxygen transport of A-site deficient $Sr_{1-x}Fe_{0.5}Co_{0.5}O_{3-\delta}$ (x = 0–0.3) membranes. *J. Membr. Sci.* **40**, 401–402 (2012).
34. A.A. Yaremchenko, C. Buysse, V. Middelkoop, F. Shijkers, A. Buekenhoudt, J.R. Frade, and A.V. Kovalevsky: Impact of sulphur contamination on the oxygen transport mechanism through $Ba_{0.5}Sr_{0.5}Co_{0.8}Fe_{0.2}O_{3-\delta}$: relevant issues in the development of capillary and hollow fibre membrane geometry. *J. Membr. Sci.* **428**, 123 (2013).
35. Yu. F. Kargin: Phase equilibrium in Bi_2O_3-NiO system. *Russ. J. Inorg. Chem.* **39**, 2079 (1994).
36. Yu. F. Kargin: Phase equilibrium in Bi_2O_3-M_2O_3 (M – Sc, In and Tl) systems. *Russ. J. Inorg. Chem.* **45**, 1553 (2000).
37. G.P. Guha, S. Kunej, and D.J. Suvorov: Phase equilibrium relations in binary system Bi_2O_3-ZnO. *J. Mater. Sci.* **39**, 911 (2004).
38. R.M. German, P. Suri, and S.J. Park: Review: liquid-phase sintering. *J. Mater. Sci.* **44**, 1 (2009).
39. V.V. Belousov: Grain boundary wetting in ceramic cuprates. *J. Mater. Sci.* **40**, 2361 (2005).
40. V.V. Belousov: Surface ionics: a brief review. *J. Eur. Ceram. Soc.* **27**, 3459 (2007).
41. V.V. Belousov: Grain boundary wetting in ceramic materials. *Colloid. J.* **66**, 121 (2004).
42. V.V. Belousov: Wetting of grain boundaries in cuprate ceramics. *Inorg. Mater.* **39**, 82 (2003).
43. V.V. Belousov: Surface energy of bismuth cuprate. *J. Supercond.* **15**, 207 (2002).
44. D.R. Clarke: Varistor ceramics. *J. Am. Ceram. Soc.* **82**, 485 (1999).
45. R.H. French: Origins and applications of London dispersion forces and Hamaker constants in ceramics. *J. Am. Ceram. Soc.* **83**, 2117 (2000).
46. V.V. Belousov and A.A. Klimashin: Catastrophic oxidation of copper: a brief review. *Metall. Mater. Trans. A* **43A**, 3715 (2012).
47. V.V. Belousov: Rapid nondiffusional penetration of oxide melts along grain boundaries of oxide ceramics. *J. Am. Ceram. Soc.* **82**, 1342 (1999).
48. V.V. Belousov: Catastrophic oxidation of metals. *Russ. Chem. Rev.* **67**, 563 (1998).
49. V.V. Belousov: Electrochemical mechanism of hot corrosion of Bi_2O_3-deposited copper. *Corros. Sci.* **52**, 68 (2010).
50. V.V. Belousov: Liquid-channel grain-boundary structures. *J. Am. Ceram. Soc.* **79**, 1703 (1996).
51. V.V. Belousov: Liquid-channel grain-boundary structures with ionic conduction. *Russ. J. Electrochem.* **31**, 1240 (1995).
52. R.J. Xie, M. Mitomo, and G.D. Zhan: Superplasticity in a fine-grained beta-silicon nitride ceramic containing a transient liquid. *Acta Mater.* **48**, 2049 (2000).
53. P. Kofstad: *Electrical Conductivity, Nonstoichiometry and Diffusion in Binary Metal Oxides* (Wiley, New York, 1972).
54. T. Bak, J. Nowotny, M. Rekas, C.C. Sorrell, P. A. Banda, and W. Wolodarski: Electrical conductivity of indium sesquioxide thin film. *J. Mater. Sci.* **13**, 571 (2002).
55. J. Feinleib and D. Adler: Band structure and electrical conductivity of NiO. *Phys. Rev. Lett.* **21**, 1010 (1968).
56. N.G. Eror and J.B. Wagner: Electrical conductivity of single crystalline nickel oxide, *Phys. Status Solidi* **35**, 641 (1969).
57. D.A. Mac Do'nail and P.W.M. Jacobs: On the lattice parameters of some sesquioxides with the fluorite structure. *J. Solid State Chem.* **84**, 183 (1990).
58. N.M. Sammes, G.A. Tompsett, H. Nafe, and F. Aldinger: Bismuth based oxide electrolytes structure and ionic conductivity. *J. Eur. Ceram. Soc.* **19**, 1801 (1999).
59. P. Shuk, H.D. Wiemhofer, and W. Gopel: Oxide ion conducting electrolytes based on Bi_2O_3. *Solid State Ion.* **89**, 179 (1996).
60. K. Laurent, G.Y. Wang, S. Tusseau-Nenez, and Y. Leprince-Wang: Structure and conductivity studies of electrodeposited δ-Bi_2O_3. *Solid State Ion.* **178**, 1735 (2008).
61. S. Hull: Superionic: crystal structures and conduction processes. *Rep. Prog. Phys.* **67**, 1233 (2004).
62. M. Yashima and D. Ishimura: Crystal structure and disorder of the fast oxide-ion conductor cubic Bi_2O_3. *Chem. Phys. Lett.* **378**, 395 (2003).
63. D. Music, S. Konstantinidis, and J.M. Schneider: Equilibrium structure of δ-Bi_2O_3 from first principles. *J. Phys.: Condens. Mater.* **21**, 175403 (2009).
64. G. Gattow and H. Schroder: Structure of high-temperature δ-Bi_2O_3. *Z. Anorg. Allg. Chem.* **318**, 176 (1962).
65. B.T.M. Willis: The anomalous behavior of the neutron reflexion of fluorite. *Acta Crystallogr.* **18**, 75 (1965).
66. C. Wagner: Theory of tarnishing process. *Z. Phys. Chem.* **21B**, 25 (1933).
67. Y. Waseda and J.M. Toguri: *The Structure and Properties of Oxide Melts* (World Scientific, Singapore, 1998).
68. A. Janotti and C.G. Van de Walle: Fundamentals of zinc oxide as a semiconductor, *Rep. Prog. Phys.* **72**, 1 (2009).
69. L. Liu, J. Xu, D. Wang, M. Jiang, S. Wang, B. Li, Z. Zhang, D. Zhao, C. X. Shan, B. Yao, and D.Z. Shen: p-Type conductivity in N-doped ZnO: the role of the N_{Zn}-V_O complex. *Phys. Rev. Lett.* **108**, 215501 (2012).
70. H. Wang, A. Feldhoff, and J. Caro: A cobalt-free oxygen-permeable membrane based on the perovskite-type oxide $Ba_{0.5}Sr_{0.5}Zn_{0.2}Fe_{0.8}O_{3-\delta}$. *Adv. Mater.* **17**, 1785 (2005).
71. A.V. Kovalevsky: Processing and oxygen permeation studies of asymmetric multilayer $Ba_{0.5}Sr_{0.5}Co_{0.8}Fe_{0.2}O_{3-\delta}$ membranes. *J. Membr. Sci.* **380**, 68 (2011).
72. J.E. Ten Elshof, H.J.M. Bouwmeester, and H. Verweiy: Oxidative coupling methane in a mixed-conducting perovskite membrane reactor. *Appl. Catal.* A **130**, 195 (1995).
73. A.A. Yaremchenko, V.V. Kharton, A.A. Valente, F.M.M. Snijkers, A.L. Cooymans, and F.M.B. Marques: Oxygen permeability, thermal expansion and stability of $SrCo_{0.8}Fe_{0.2}O_{3-\delta}$ – $SrAl_2O_4$ composites. *Solid State Ion.* **178**, 1205 (2007).
74. V.V. Kharton and A.A. Yaremchenko: Perovskite-type oxides for high-temperature oxygen separation. *J. Membr. Sci.* **163**, 307 (1999).
75. H.W. Brinkman, H. Kruidhof, and A.J. Burggraaf: Mixed conductivity yttrium-barium-cobalt-oxide for high oxygen permeation. *Solid State Ion.* **68**, 173 (1994).
76. J.W. Stevenson, T.R. Armstrong, R.D. Carneim, L.P. Pederson, and W.J. Weber: Electrochemical properties of mixed-conducting perovskites $La_{1-x}M_xCo_{1-y}Fe_yO_{3-\delta}$ (M – Sr, Ba and Ca). *J. Electrochem. Soc.* **143**, 2722 (1996).

https://doi.org/10.1557/mrc.2013.41 Published online by Cambridge University Press

77. M.A. Pena and J.L.G. Fierro: Chemical structures and performance of perovskite oxides. *Chem. Rev.* **101**, 1981 (2001).
78. S. Lee: Mechanical properties and structure stability of perovskite type, oxygen-permeable, dense membranes. *Desalination* **193**, 236 (2006).
79. J. Sunarso, S. Baumannb, J.M. Serrac, W.A. Meulenbergb, S. Liua, Y.S. Lind, and J.C. Diniz da Costaa: Mixed ionic-electronic conducting (MIEC) ceramic-based membranes for oxygen separation. *J. Membr. Sci.* **320**, 13 (2008).
80. A.V. Chadwick: Nanotechnology: solid progress in ion conduction. *Nature* **408**, 925 (2000).
81. V.V. Belousov: High temperature solid/melt nanocomposites. *JETP Lett.* **88**, 297 (2008).

https://doi.org/10.1557/mrc.2013.41 Published online by Cambridge University Press